



HHS Public Access

Author manuscript

Stem Cells. Author manuscript; available in PMC 2016 December 01.

Published in final edited form as:

Stem Cells. 2015 December ; 33(12): 3581–3595. doi:10.1002/stem.2098.

Pharyngeal satellite cells undergo myogenesis under basal conditions and are required for pharyngeal muscle maintenance

Matthew E. Randolph¹, Brittany L. Phillips¹, Hyo-Jung Choo¹, Katherine E. Vest¹, Yandery Vera¹, and Grace K. Pavlath¹

¹Department of Pharmacology, Emory University, Atlanta, GA 30322, USA

Abstract

The pharyngeal muscles of the nasal, oral, and laryngeal pharynxes are required for swallowing. Pharyngeal muscles are preferentially affected in some muscular dystrophies yet spared in others. Muscle stem cells, called satellite cells, may be critical factors in the development of pharyngeal muscle disorders; however, very little is known about pharyngeal satellite cells (PSC) and their role in pharyngeal muscles. We show that PSC are distinct from the commonly studied hindlimb satellite cells both transcriptionally and biologically. Under basal conditions PSC proliferate, progress through myogenesis, and fuse with pharyngeal myofibers. Furthermore, PSC exhibit biologic differences dependent on anatomic location in the pharynx. Importantly, PSC are required to maintain myofiber size and myonuclear number in pharyngeal myofibers. Together, these results demonstrate that PSC are critical for pharyngeal muscle maintenance and suggest that satellite cell impairment could contribute to pharyngeal muscle pathology associated with various muscular dystrophies and aging.

Keywords

pharynx; satellite cells; myofiber; myonuclear turnover; muscle maintenance

Introduction

Muscular dystrophies are a group of degenerative muscle diseases that impair different subsets of skeletal muscles depending on the specific type of muscular dystrophy [1–8]. One muscle group differentially affected in muscular dystrophies is found in the pharynx.

Corresponding author G.K. Pavlath: Emory University, Department of Pharmacology, 1510 Clifton Rd, Room 5027, Atlanta, GA 30322, USA. gpavlat@emory.edu.

Author Contributions:

M. E. Randolph: Conception and design, financial support, collection and assembly of data, data analysis and interpretation, manuscript writing, final approval of manuscript

B. L. Phillips: Collection and assembly of data, data analysis and interpretation, manuscript writing, final approval of manuscript

H. J. Choo: Collection and assembly of data, data analysis and interpretation, manuscript writing, final approval of manuscript

K. E. Vest: Collection and assembly of data, data analysis and interpretation, manuscript writing, final approval of manuscript

Y. Vera: Collection and assembly of data, data analysis and interpretation, final approval of manuscript

G. K. Pavlath: Conception and design, financial support, administrative support, provision of study materials, data analysis and interpretation, manuscript writing, final approval of manuscript

Disclosure of Potential Conflicts of Interest

The authors report no potential conflicts of interest.

Pharyngeal muscles are a vital group of seven muscles involved in swallowing. They are non-somitic in origin, arising from the cranial mesoderm of the third and fourth pharyngeal arches in vertebrates [9, 10]. These muscles surround the nasal, oral, and laryngeal pharynxes and include the palatopharyngeus, stylopharyngeus, salpingopharyngeus, superior and middle pharyngeal constrictors, cricopharyngeus, and thyropharyngeus muscles [11–16]. One type of muscular dystrophy in which pharyngeal muscles are pathologically affected is oculopharyngeal muscular dystrophy (OPMD), a late onset autosomal dominant disease caused by a polyalanine expansion in the N-terminal domain of the ubiquitously expressed polyadenylate-binding protein nuclear 1 (PABPN1) protein [6, 17, 18]. Interestingly, the associated muscle stem cells of pharyngeal muscles are also pathologically affected in OPMD patients [19].

Muscle stem cells, called satellite cells, are a heterogeneous cell population that is responsible for repair of muscle tissue [20]. In hindlimb skeletal muscle, satellite cells are mitotically quiescent under basal conditions [20]. When muscle tissue is damaged or injured, satellite cells proliferate, differentiate, migrate, adhere and fuse to each other or existing myofibers to form multi-nucleated myofibers while a subset of satellite cells undergo self-renewal to maintain a quiescent stem cell population [20]. Considering that pharyngeal satellite cells are altered in OPMD and that satellite cells in other skeletal muscles are thought to play a role in the pathology of muscle diseases such as Duchenne muscular dystrophy [21], congenital muscular dystrophy 1A [22], Emery-Dreifuss muscular dystrophy [23], and facioscapulohumeral muscular dystrophy [24, 25] we addressed whether pharyngeal satellite cells may have unique biological properties that make them susceptible to disease-inducing conditions.

In this study, we analyzed the biologic properties of PSC and their contribution to pharyngeal muscle maintenance. We characterized PSC *in vivo* in a region-dependent manner: analyzing PSC of the palatopharyngeus muscle (nasal and oral pharynx) along with the cricopharyngeal and thyropharyngeal muscles (laryngopharynx). Somite-derived satellite cells from hindlimb muscles were used for comparison. We found that PSC are distinct from hindlimb satellite cells both transcriptionally and biologically. PSC undergo constitutive myogenesis and, unlike hindlimb satellite cells [26–30], are required to maintain myofiber size and myonuclear number in pharyngeal myofibers. Our findings provide new insights into the biology of PSC and pharyngeal muscles that may be important in understanding why certain muscular dystrophies target muscles of the pharynx.

Materials and Methods

Mice

Adult male mice, between 2–4 months of age, were used unless noted otherwise. C57BL/6 were purchased from Charles River Laboratories. *Myf5^{nLacZ/+}* (*Myf5* nLacZ) and *Pax7^{CreERTM/CreERTM}* (*Pax7^{CreERTM}*) mice were obtained from S. Tajbakhsh [31] and C. Keller [32], respectively. Duchenne muscular dystrophy model mice containing a dystrophin-deficient allele with a splice site mutation in exon 23, C57BL/10ScSn-Dmd^{mdx/J} (*Mdx*) [33], were purchased from Jackson Laboratories. Rosa26-CAG-tdTomato [34] and Rosa26-DTA176 mice [35] were also purchased from Jackson Laboratories. Homozygous

Pax7^{CreERTM/CreERTM} male mice were crossed with either homozygous *Rosa^{DTA176/DTA176}* (DTA) females to obtain *Pax7^{CreERTM/+}; Rosa^{DTA176/+}* (DTA-Pax7^{CreERTM}) mice for satellite cell ablation experiments, or with homozygous *Rosa^{tdTomato/tdTomato}* (tdTom) to obtain *Pax7^{CreERTM/+}; Rosa^{tdTomato/+}* (tdTom-Pax7^{CreERTM}) mice to fluorescently label myogenic cells after tamoxifen treatment. Genomic recombination and removal of floxed stop sequences were induced in male DTA-Pax7^{CreERTM} and tdTom-Pax7^{CreERTM} mice at 8 weeks-of-age. Tamoxifen, 1 mg (Sigma) per 10 grams body weight, was injected intraperitoneally once daily for five days. Flow cytometry was utilized to determine the recombination efficiency in both DTA-Pax7^{CreERTM} and tdTom-Pax7^{CreERTM} mice. Experiments were performed in accordance with approved guidelines and ethical approval from Emory University's Institutional Animal Care and Use Committee and in compliance with the National Institutes of Health.

Dissection of Pharyngeal Tissue

CO₂ asphyxiation was utilized to euthanize mice immediately prior to tissue collection. Pharyngeal tissue dissection was performed as previously described [16]. Histologic samples included pharyngeal tissue extending from the soft palate caudally to the cranial aspects of the trachea and esophagus. The larynx and trachea were excluded from pharyngeal samples collected for isolation of myogenic cells.

Flow Cytometry and Fluorescence Activated Cell Sorting

For analysis via flow cytometry, mononucleated cells were isolated from pharyngeal and hindlimb (gastrocnemius and quadriceps) muscles as previously described [36, 37]. Briefly, pharyngeal and hindlimb muscles were minced and digested in Dulbecco's Modified Eagle's Medium (DMEM) (Mediatech) containing 1 mg/ml pronase (Calbiochem), 25 mM HEPES at 37°C for 45 minutes or 1 hour, respectively. Cellular preps were applied to Percoll (GE Healthcare) gradients of 20 and 60% for enrichment of myogenic cells and removal of red blood cells [38]. Digested muscles were washed with DMEM and mononucleated cells collected using 100 μ m Steriflip filtration systems (Milipore) prior to antibody labeling.

For analysis and collection via FACS, pharyngeal and hindlimb (gastrocnemius and quadriceps) muscles were minced and digested in Ham's F10 media (Hyclone) containing 500 units/ml collagenase II (Gibco) and 10% fetal bovine serum (FBS) at 37°C while shaken at 65 rpm for 90 minutes. Digested muscles were then rinsed with Ham's F10 media containing 10% FBS, 100 U/ml penicillin G, and 100 μ g/ml streptomycin (P/S), followed by a second digestion using 100 units/ml collagenase II, 1 unit/ml dispase (Gibco) in Ham's F10 media containing 10% FBS, P/S under the same conditions for 30 minutes. Digested muscles were washed with 0.1 M Dulbecco's phosphate-buffered saline, pH 7.3 (PBS) (Gibco) and mononucleated cells collected using 100 μ m Steri-Flip filtration systems (Milipore).

Isolated cells were resuspended in PBS containing 1% bovine serum albumin (BSA) for antibody labeling. Dead cells were identified using 5 μ g/ml propidium iodide (PI). Myogenic cells, identified as PI⁻/Sca1⁻/CD31⁻/CD45⁻/ α 7-integrin⁺ (Lin⁻ α 7-integrin⁺) [39] were isolated and collected using a FACSAria II (Becton-Dickinson) at the Emory

University School of Medicine Core Facility for Flow Cytometry. Analyses of flow cytometry data were performed using FlowJo (version 9.5.2). Isolated myogenic cells were then processed for *in vitro* cultures, immunofluorescent staining, or RNA extraction. Primary antibodies included rat anti-CD31-Phycoerythrin (PE) (0.5 $\mu\text{g}/\text{ml}$; eBioscience) and rat CD45-PE (0.5 $\mu\text{g}/\text{ml}$; BD Pharmingen), rat Sca-1-PE-Cy7 (0.05 $\mu\text{g}/\text{ml}$; BD Pharmingen), rat $\alpha 7$ -integrin-AlexaFluor649 (1 $\mu\text{g}/\text{ml}$; AbLabs) and appropriate rat isotype control antibodies (BD Pharmingen).

Immunohistochemistry/Immunofluorescence

All muscle tissues were cryofrozen in Tissue Freezing Medium™ (Triangle Biomedical Sciences) and stored at -80°C . Tissue sections of 10 μm thickness were collected every 80 or 200 μm using a Leica CM1850 cryostat to analyze pharyngeal and hindlimb muscles, respectively. Tissue sections from Myf5-nLacZ mice were fixed in 4% paraformaldehyde, 0.1 M NaP_i (pH 7.2), 0.5% glutaraldehyde, followed by a PBS wash, and then incubated at 37°C with 1 mg/ml X-gal in dimethylformamide for 12–18 hours to identify β -galactosidase activity. Peripheral and centrally localized β -gal positive nuclei were quantified using ImageJ 1.43u.

For immunostaining of tissue sections for dystrophin and BrdU, the M.O.M. Kit (Vector Laboratories Inc.) was used to block endogenous Fc receptor binding sites followed by a 1 hour incubation with 5% goat serum, 5% donkey serum, 0.5% BSA, 0.20% Triton-X 100 in PBS (blocking buffer). Sections were then labeled with blocking buffer containing primary antibodies or appropriate isotype controls overnight at 4°C . Successive washes in 0.25% Tween 20 in PBS (PBS-T) were followed by another 60 minute incubation with appropriate secondary antibodies at room temperature. Sections were then washed with PBS-T and nuclei labeled with 4',6-diamidino-2-phenylindole (DAPI) (1 $\mu\text{g}/\text{ml}$) in PBS. Primary antibodies included rat anti-BrdU (2 $\mu\text{g}/\text{ml}$, clone BU1/75 (ICR1), Accurate Chemical and Scientific), and mouse anti-dystrophin (13.5 $\mu\text{g}/\text{ml}$, clone MANDYS8, Sigma). Immunostaining for BrdU was performed on post-dystrophin immunostained sections as follows. Sections were fixed with 2% paraformaldehyde in PBS for 10 minutes, followed by a PBS wash, 2 minute chilled acetone treatment, and another PBS wash. Subsequently, sections were treated with 1 N HCl in PBS at 45°C for 20 minutes and immediately neutralized with a 0.1 M sodium tetraborate/boric acid buffer, pH 8.5, for 8 minutes at room temperature. Additional tissue blocking was performed with 0.3 M glycine in PBS for 30 minutes and 24 $\mu\text{g}/\text{ml}$ AffiniPure goat α -mouse IgG F(ab')₂ (Jackson ImmunoResearch)/ml PBS-T at room temperature for 1 hour. Sections were then immunostained for BrdU following the standard immunostaining protocol described above.

For immunostaining of Pax7 and laminin, tissue sections from hindlimb (tibialis anterior) and pharyngeal muscles were fixed in freshly prepared 4% paraformaldehyde (Electron microscopy sciences), followed by PBS washes. Sections were heated in citrate buffer (10mM sodium citrate, 0.05% Tween-20, pH 6.0) for antigen retrieval with a pressure cooker (Cuisinart model CPC-600) for 6 minutes. Before immunostaining of tissue sections, the M.O.M. Kit (Vector Laboratories Inc.) was used to block endogenous Fc receptor binding sites followed by a 1 hour incubation with 10% goat serum, 10% donkey serum,

0.5% BSA, 1% Triton-X 100 in PBS. Sections were then labeled with mouse anti-Pax7 (3.8 $\mu\text{g}/\text{ml}$, Developmental Hybridoma Studies Bank) and rabbit anti-laminin (2 $\mu\text{g}/\text{ml}$, Sigma) antibodies or IgG isotype controls overnight at 4°C. Successive washes in PBS-T were followed by incubating in 0.3% H_2O_2 for 10 minutes to block endogenous peroxidase. Sections were incubated for 20 minutes with biotinylated goat-anti-mouse $\text{F}(\text{ab}')_2$ IgG fragments (1 $\mu\text{g}/\text{ml}$, Jackson ImmunoResearch) for Pax7 imaging. A TSA (Tyramide Signal Amplification; Perkin Elmer) Green kit was used for subsequent steps. Sections were incubated in TNB (Tris-NaCl blocking buffer) for 20 minutes followed by incubation with HRP-conjugated streptavidin diluted 1:200 in TNB for 20 minutes. Finally, signals were amplified by TSA Green diluted 1:300 in amplification buffer for 5 minutes. After further washes with PBS-T, sections were incubated with AF594-donkey anti-rabbit $\text{F}(\text{ab}')_2$ IgG fragments for 40 minutes for laminin imaging. Sections were then washed using PBS-T and nuclei labeled with DAPI in PBS. Sections were mounted with Vectashield (Vector lab).

Immunofluorescent staining for Pax7 was performed on $\text{Lin}^- \alpha 7\text{-integrin}^+$ and $\text{Lin}^- \alpha 7\text{-integrin}^-$ cells collected via FACS. Cytospun cells were incubated with the M.O.M. kit and blocking buffer sequentially for one-hour intervals. Cells were incubated with mouse anti-Pax7 (7.5 $\mu\text{g}/\text{ml}$, Developmental Studies Hybridoma Bank) at RT for one hour, followed by PBS-T washes, and further labeled using biotinylated goat-anti-mouse $\text{F}(\text{ab}')_2$ IgG fragments. Pax7 staining was visualized using the TSA Green kit, as described above. Cells were then washed with PBS-T and nuclei labeled with DAPI. Samples were then mounted with Vectashield for imaging.

Myofiber cross-sectional areas of 929–1505 myofibers were quantified on hematoxylin (Thermo Scientific) and eosin (Sigma-Aldrich) stained sections using ImageJ 1.43u. For all tissue section studies, four, five, or six representative sections imaged at 200 \times magnification were analyzed from muscles of the nasal, oral, and laryngeal pharynx, respectively, while four sections were analyzed per tibialis anterior muscle. Images were acquired at 23°C using an Axioplan microscope with a 0.5 NA 20 \times Plan-Neofluar objective (Carl Zeiss MicroImaging, Inc.) and charge-coupled device camera (Carl Zeiss MicroImaging, Inc.) with Scion Image 1.63 (Scion Corp.). Photoshop CS4 (Adobe) was used to globally process all images for contrast, size, and brightness. Data were blinded for analysis.

Single myofiber isolation and imaging

Single myofibers were isolated, as previously described [40] from pharyngeal muscles of mice 2–5, 12, or 18 months-of-age. Briefly, pharyngeal muscles were dissected and digested with gentle agitation in 4.5 mg/ml glucose, 100 U/ml penicillin G, 100 $\mu\text{g}/\text{ml}$ streptomycin, 25 mM HEPES in DMEM containing either 400 or 800 U/ml collagenase type I (Worthington), respectively, at 37°C for 90 minutes. Single myofibers were washed 3 times with collagenase-free DMEM prior to manual extraction onto clean 100-mm plates. Myofibers were then individually transferred onto 10% growth factor-reduced Matrigel (BD Biosciences) coated 24-well plates, and centrifuged at 1100 \times g to enhance myofiber adherence. Myofibers were then fixed with 2% formaldehyde in PBS and stained with DAPI. Pharyngeal muscles from 18-month-old mice required digestion with 1600 U collagenase type I/ml DMEM media. Single myofiber images were visualized at 23°C using

an Axiovert 200M microscope with a 0.3 NA 10× Plan-Neofluar objective (Carl Zeiss MicroImaging, Inc.). Images were captured with a QImaging camera and OpenLab 5.5.2 (Improvision) software. Myofiber diameter, length, and nuclear number were quantified using ImageJ 1.43u. Photoshop CS4 (Adobe) was used to globally process all images for contrast and brightness. Between 929–1505 myofibers were pooled and analyzed from 5 mice per age group for each muscle.

Evans Blue Assay

C57BL/6 and Mdx mice received an intraperitoneal injection of 1% Evans Blue Dye (Sigma) suspended in sterile PBS at a volume of 10 μ l/gram body weight. Mice were euthanized via CO₂ asphyxiation 24 hours post-injection and immediately prior to dissection and collection of tibialis anterior and pharyngeal muscles for cryosectioning. Tissues were sectioned at a thickness of 10 μ m and analyzed for the presence of Evans Blue fluorescence within myofibers. Images were acquired at 23°C using an Axioplan microscope with a 0.8 NA 25× Plan-Neofluar objective (Carl Zeiss MicroImaging, Inc.) and charge-coupled device camera (Carl Zeiss MicroImaging, Inc.) with Scion Image 1.63 (Scion Corp.). Photoshop CS4 (Adobe) was used to globally process all images for contrast, size, and brightness.

In Vivo BrdU Assays

To compare the proliferative and fusogenic abilities of pharyngeal and hindlimb satellite cells *in vivo*, 5-bromo-2'-deoxyuridine (BrdU) assays were performed. Three-month-old male C57BL/6 mice were injected with 10 μ g BrdU (Sigma)/gram body weight intraperitoneally every 12 hours. To assess proliferation, mice were injected over a 48-hour period. To assess fusion, injections were given for 7 days followed by 7 days of 0.8% BrdU in 2% sucrose water.

Proliferation assay—Pharyngeal and gastrocnemius muscles of 3–5 mice were collected forty-eight hours post-initial BrdU injection. Mononucleated cells were isolated from pooled muscles, selected with Percoll gradients, immunostained, fixed with formalin, and analyzed using flow cytometry, as described above. Proliferating myogenic cells were identified as BrdU⁺, Sca1⁻/CD31⁻/CD45⁻/ α 7-integrin⁺. BrdU immunostaining was performed using the FITC BrdU Flow Kit (1:200, BD Pharmingen™). As a positive control for proliferating cells, muscle injuries were performed in anesthetized mice by injecting 40 μ l of 1.2% BaCl₂ into gastrocnemius muscles as previously described [41] two days prior to collection.

Fusion assay—Pharyngeal and tibialis anterior muscles were collected 14 days post-initial BrdU injection as described for tissue sectioning. Representative tissue sections were immunostained to detect dystrophin and BrdU as described above. The number of intrafiber BrdU⁺ myonuclei/100 myofibers was quantified using ImageJ 1.43u. Samples were blinded for analysis.

Microarray

Myogenic cells from pharyngeal and hindlimb (gastrocnemius and quadriceps) muscles were isolated, sorted using FACS, and collected from 10–30 mice per experiment. Samples were sent to the Emory University Integrated Genomics Core facility for total RNA isolation

using Qiagen miRNEasy kit with on-column DNase treatment followed by one round of amplification using NuGEN's WT-Ovation Pico amplification kit. Analysis of genomic gene expression was performed using an Illumina Mouse WG-6 v2.0 Expression BeadChip. Data was extracted using the Illumina HiScan Scanner and iScan control software. Illumina Genome Studio 2011.1 software suite was used to normalize probe level intensity data with background correction using manifest MouseWG-6_V2_0_R1_11278593_A.txt. Detection p-values were calculated as the proportion of negative control probes with expression greater than the regular probe in question using Partek Genome Studio. The data discussed in this publication have been deposited in NCBI's Gene Expression Omnibus [42] and are accessible through GEO Series accession number GSE69418 (<http://www.ncbi.nlm.nih.gov/geo/query/acc.cgi?acc=GSE69418>).

Data were further analyzed using both MetaCore Genego (<https://portal.genego.com>; Thomson Reuters) and Gene Set Enrichment Analysis (www.broadinstitute.org/gsea/index.jsp; Broad Institute).

Real-time PCR

Myogenic cells from pharyngeal and hindlimb (gastrocnemius and quadriceps) muscles were isolated, sorted using FACS, and collected from 10–30 mice per experiment. Total RNA was isolated using the PicoPure RNA Isolation Kit (Applied Biosystems) from samples of 150,000–200,000 pooled cells each. cDNA was generated from total RNA via a reverse transcriptase reaction using M-MLV reverse transcriptase (Invitrogen) and random hexamer primers. cDNA was then amplified using the SYBR Select Master Mix reagent (Applied Biosystems) and 2.5 μ M of each primer. All RNA samples were tested for DNA contamination by PCR. Primer sequences were: MyoD (F: 5'-GCCCGCGCTCCAAGTCTGAT-3' and R: 5'-CCTACGGTGGTGCGCCCTCTGC-3'); Pax7 (F: 5'-CACCCGGGGACAGAGGAAGAT-3' and R: 5'-GAGAGGGCGGGTACAAGGAAGAC-3'). All other primers were purchased from Qiagen's RT² qPCR Primer Assay library. Real-time PCR reactions were performed and analyzed with a StepOnePlus Real Time PCR System (Applied Biosystems), using GAPDH or 18S as an internal control. Fold change of gene expression was determined using the $\Delta\Delta$ Ct method [43]. Three to four independent experiments were performed and analyzed in duplicate.

Clonal Expansion Assay

Conditioned media (CM), collected from either primary hindlimb or pharyngeal muscle cell cultures, contained 20% FBS, 100 U/ml penicillin, 100 μ g/ml streptomycin, 5 ng/ml basic fibroblast growth factor (bFGF) in Ham's F10 media. Any contaminating cells were removed through sterile syringe filtration with a 0.20 μ m filter (Corning). Mononucleated cell suspensions obtained from pharyngeal and hindlimb (gastrocnemius and quadriceps) muscles of C57BL/6 mice were then subjected to FACS, as previously described. Sorted myogenic cells were plated at clonal densities of 100–250 cells/100 mm collagen-coated plates and grown in CM diluted 1:1 with Ham's F10 media containing 20% FBS, 100 U/ml penicillin, 100 μ g/ml streptomycin and 5 ng/ml bFGF at 37°C for 8 days prior to 2%

paraformaldehyde fixation. Cells were then counterstained with hematoxylin (Thermo Scientific). Bright field images were acquired at 8× magnification using a Leica MZFL III microscope (Leica, Inc.) with a Planapo 1.0× objective (Leica, Inc.). Images were captured with a QImaging Retiga Exi Fast 1394 camera and QCapture Suite version 2.70 (Quantitative Imaging Corp.) software. Analyses of cell number per colony and number of clonal colonies were performed on 264 clones. Photoshop CS4 (Adobe) was used to globally process all images for contrast and brightness.

Statistical Analyses

Data were analyzed for statistical significance using GraphPad Prism version 5 for Macintosh (GraphPad Software). For all statistical tests, a 0.05 level of confidence was considered statistically significant. When comparing two groups, data were analyzed by unpaired Students *t* test. To determine significance among multiple groups, data were analyzed using one-way ANOVA with Bonferroni's posttest. Nonparametric data were analyzed using the Kruskal-Wallis test with Dunn's posttest to identify statistical differences between sample distributions.

Results

Pharyngeal muscles contain larger numbers of activated satellite cells than hindlimb muscles in the absence of overt injury

To date, satellite cells of adult mouse pharyngeal muscles, which arise from the third and fourth pharyngeal arches during development, have not been studied in depth, unlike satellite cells of muscles arising from the first and second pharyngeal arches ([44] [45] [46]). Therefore, to gain insights into PSC we initially analyzed their numbers in pharyngeal muscles. The pharynx can be subdivided into three distinct regions (nasal, oral, and laryngeal)(Fig. 1A). Each region and their associated muscles vary in both location and function. We recently reported that muscles within the nasal, oral, and laryngeal regions of the pharynx are differentially affected by aging and disease [16]. Therefore, all histologic studies were analyzed based on pharyngeal localization. To analyze satellite cell numbers throughout each region of the pharynx, we used a mouse model that expresses nuclear-localized β -galactosidase (β -gal) under the promoter of the myogenic transcription factor Myf5 (Myf5-nls-LacZ), which is commonly used to mark both quiescent and activated satellite cells within muscle tissues [31, 47, 48]. X-gal staining of hindlimb and pharyngeal muscle sections from 3–5 month old mice (Fig. 1B) revealed significantly increased numbers of β -gal⁺ cells (Fig. 1C), located at the periphery of myofibers throughout the oral and laryngeal pharynxes compared to hindlimb muscle. To differentiate between quiescent and activated satellite cells, we immunostained pharyngeal muscle sections for paired box protein 7 (Pax7), a marker of quiescent satellite cells (Fig. 1E) [49]. Pax7⁺ satellite cell numbers were significantly decreased in the nasopharynx while increased in the laryngopharynx compared to hindlimb muscle (Fig. 1F). The increased numbers of Pax7⁺ satellite cells in the murine laryngopharynx are consistent with recent immunohistologic studies of human cricopharyngeal muscles [50]. Most strikingly, our Myf5- β -gal data demonstrate that the majority of satellite cells are activated in pharyngeal muscles.

We then analyzed whether muscle damage was present in pharyngeal muscles, which would induce a regenerative response resulting in increased numbers of activated satellite cells. We observed no signs of myofiber degeneration in sections despite the fact that Myf5-nls-LacZ pharyngeal myofibers contained a high incidence of centrally located β -gal⁺ myonuclei compared to hindlimb muscles (Fig. 1D), suggestive of recent satellite cell fusion with myofibers [47]. To confirm that no overt myofiber damage was present, we injected mice with Evans Blue and muscle sections were analyzed for fluorescence. Damaged myofibers were identified by the presence of Evans Blue dye within the myofiber, as seen in mdx mice, which are characterized by damaged myofiber membranes due to the loss of dystrophin (Supp. Fig. 1). However, no Evans Blue positive myofibers were observed in any of the wild-type pharyngeal muscles examined (Supp. Fig. 1). Therefore, the increase in activated satellite cell numbers in pharyngeal muscles could not be attributed to myofiber damage, suggesting that alternative mechanisms are responsible for the increased satellite cell numbers and centrally located myonuclei of pharyngeal muscles.

Identification of pharyngeal satellite cells

To gain further insights into the biology of pharyngeal satellite cells, we initially confirmed which molecular markers would reliably identify these cells *in vivo*. Satellite cells in different muscles can be identified using multiple molecular markers [39, 51–57], but such markers have not been validated for PSC. Hindlimb satellite cells (LSC) have previously been identified as cells expressing α 7-integrin that are not of endothelial, hematopoietic, or fibro-adipogenic progenitor lineages (CD31⁻ CD45⁻ Sca1⁻) [39]. To validate whether these markers also identified PSC, pharyngeal muscles were enzymatically dissociated to yield mononucleated cells. Analysis by flow cytometry revealed a distinct sub-population of lineage-negative (CD31⁻ CD45⁻ Sca1⁻), α 7-integrin expressing (Lin⁻ α 7-integrin⁺) cells present within pharyngeal tissue (Fig. 2A). To confirm the myogenic identity of pharyngeal Lin⁻ α 7-integrin⁺ cells, two different methods were used to confirm expression of Pax7 [49] (Fig. 2B–D). Over 90% of FACS-sorted pharyngeal Lin⁻ α 7-integrin⁺ cells were positive for Pax7 via immunofluorescence *in vitro* (Fig. 2B,C). To confirm these results, a tamoxifen-inducible Cre/LoxP system was utilized. Mice expressing a tamoxifen-inducible Cre recombinase under the endogenous *Pax7* promoter (Pax7^{CreERTM}) [32], were crossed with mice containing the floxed fluorescent reporter *Rosa26-tdTomato* allele (tdTom) [34] to visualize satellite cells *in vivo*. Over 90% of pharyngeal Lin⁻ α 7-integrin⁺ cells from tamoxifen treated tdTom-Pax7^{CreERTM} heterozygotes expressed tdTomato (Fig. 2D), further confirming that Lin⁻ α 7-integrin⁺ labeling identifies Pax7⁺ satellite cells from pharyngeal muscles.

Pharyngeal satellite cells proliferate in the absence of induced injury

Satellite cells of some craniofacial muscles, such as extraocular muscles, proliferate at a basal level in the absence of injury, in contrast to the quiescent phenotype of LSC [58–61]. Considering that overt muscle injury did not explain the large number of PSC or the centrally located myonuclei throughout the pharynx, we tested whether PSC were proliferating in the absence of induced injury. Bromodeoxyuridine (BrdU) assays were performed in both young and mature C57BL/6 mice to label proliferating cells. Mice received BrdU injections every twelve hours for two days (Fig. 3A). On day three, hindlimb

and pharyngeal muscles were collected, mononucleated cells isolated, and myogenic ($\text{Lin}^- \alpha 7\text{-integrin}^+$) cells analyzed via flow cytometry for evidence of BrdU labeling (Fig. 3B). At 2–5 months of age, we observed a trend towards increased satellite cell proliferation in the pharynx (Fig. 3C), and by 12 months of age, the percentage of proliferating satellite cells was significantly increased by ~30 fold in pharyngeal muscle compared to hindlimb (Fig. 3C). In sharp contrast to quiescent hindlimb satellite cells, myogenic cells from pharyngeal muscle demonstrated robust proliferation in the absence of induced injury suggesting that basal satellite cell proliferation is a characteristic of pharyngeal muscles.

The basal proliferation of pharyngeal satellite cells could be in response to signals from the pharyngeal niche and/or an intrinsic property of PSC. To examine whether the proliferative SC phenotype in pharyngeal muscles was intrinsic to PSC, satellite cells were isolated and sorted using Fluorescence Activated Cell Sorting (FACS) from both hindlimb and pharyngeal muscles. Sorted myogenic cells were plated at clonal densities and grown for 8 days in the absence of the pharyngeal muscle niche. Cultures were then fixed and stained with hematoxylin to identify nuclei. We identified highly proliferative cells as clones that produced colonies numbering more than 300 cells. While the majority of pharyngeal clones were similar in size to those of the hindlimb, 17% of pharyngeal colonies contained more than 300 cells, compared to only 6% of hindlimb colonies (Fig. 3D, Supp. Fig. 2). These data suggest that a highly proliferative subpopulation of PSC exists in pharyngeal muscles under basal conditions, thus indicating that proliferation is an intrinsic property of some PSC.

Proliferating pharyngeal satellite cells progress through the myogenic lineage

Following activation and proliferation, satellite cells typically progress through the myogenic lineage, contributing new myonuclei to muscle fibers [20]. However, impaired differentiation [46] or cell death [62] can prevent myogenic lineage progression. The increased incidence of centrally localized myonuclei in pharyngeal muscles (Fig. 1D) suggested that satellite cell fusion with myofibers does occur. To definitively test whether proliferating PSC progressed through the myogenic lineage *in vivo*, proliferating cells were labeled with BrdU over a two-week period to allow for fusion of BrdU⁺ cells into myofibers (Fig. 3E). During myogenic differentiation, satellite cells exit the cell cycle and are post-mitotic. Therefore, any BrdU⁺ myonucleus located within a myofiber would indicate recent fusion of a proliferating satellite cell. We analyzed pharyngeal muscle sections for the presence of BrdU⁺ myonuclei within dystrophin immunostained myofibers (Figure 3F). The number of intra-fiber BrdU⁺ nuclei was significantly elevated in myofibers of the oral and laryngeal pharynxes relative to those within hindlimb muscle (Fig. 3G). This result indicates that the proliferative satellite cells of pharyngeal muscles progress through the myogenic lineage and contribute new myonuclei to pharyngeal myofibers.

Pharyngeal and hindlimb satellite cells are transcriptionally distinct

To address potential molecular mechanisms involved in the constitutive myogenesis of PSC, we analyzed steady-state RNA levels of sorted $\text{Lin}^- \alpha 7\text{-integrin}^+$ cells using both quantitative real-time PCR (qRT-PCR) and microarray. qRT-PCR was utilized to analyze transcript levels of several transcription factors involved in craniofacial muscle development

and myogenesis. *Pax7*, *Myf5*, *MyoD*, *Myogenin*, and *Pitx2* transcripts were all decreased in PSC (Fig. 4A) relative to LSC, *Pax3* was not detected in PSC, while *Tcf21* was expressed only in PSC (data not shown). These data demonstrate a unique transcription profile of myogenic regulatory factors in PSC. Principal component analysis of microarray data revealed distinct expression profiles in pharyngeal versus hindlimb satellite cells (Fig. 4B). Furthermore, the steady-state levels of 964 pharyngeal transcripts were differentially expressed by ≥ 1.5 fold. These included 478 up-regulated and 486 down-regulated transcripts (Supp. Table 1 and Fig. 4C). Consistent with our *in vivo* data, analysis of PSC transcripts revealed an enrichment of genes involved in regulation of cell proliferation (GO process: 0042127; Fig. 4D). Interestingly, we found increased expression of several cytokine and chemokine transcripts in PSC, including *Lif*, *Ccl2*, *Ccl17*, *IL6*, and *IL6Ra*, all of which are involved in satellite cell proliferation and/or differentiation [63–69]. qRT-PCR analysis confirmed increased expression of *Lif*, *Ccl2*, and *IL6* in PSC relative to LSC (Fig. 4E). Together, these data demonstrate that PSC have a distinct molecular signature from those of hindlimb muscles, which could contribute to their increased proliferation and myogenic lineage progression.

Pharyngeal satellite cells are required to maintain myonuclear number in pharyngeal muscles

Our data show that PSC are transcriptionally distinct from LSC, highly proliferative, and undergo myogenesis under basal conditions. Considering the continuous myonuclear addition occurring in pharyngeal muscles, myonuclear numbers within pharyngeal myofibers would be predicted to increase over time. To test this hypothesis, we isolated individual myofibers from both hindlimb and pharyngeal muscles, stained myofibers with DAPI to visualize nuclei (Fig. 5A), and compared myonuclear numbers using three independent metrics from mice at various ages. No increase of myonuclear number was observed across the studied age range (Fig. 5B–D). These data, in conjunction with the presence of a proliferative satellite cell population, suggest that pharyngeal muscles undergo active myonuclear turnover in the absence of induced injury. To directly test whether myonuclear loss was occurring in pharyngeal myofibers, we crossed the *Pax7^{CreERTM}* mouse with mice containing the floxed truncated diphtheria toxin A-176 allele in the *Rosa26* locus (*DTA-Pax7^{CreERTM}*) [35] to induce ablation of *Pax7⁺* satellite cells *in vivo* (Fig. 5E). When *Pax7⁺* cells were ablated following tamoxifen-induced expression of DTA, a 93% loss of *Lin⁻ α 7-integrin⁺* cells was observed (Fig. 5F, Supp. Fig. 3). We hypothesized that removing ~93% of all satellite cells from pharyngeal muscles would severely impair myonuclear addition and, if myonuclear turnover were occurring in pharyngeal muscle, loss of myonuclei would be evident over time. Therefore, we collected pharyngeal muscles from *DTA-Pax7^{CreERTM}* mice 4 months following treatment with either vehicle or tamoxifen (Fig. 5E). Muscle sections were labeled for dystrophin to identify pharyngeal myofibers and counterstained with DAPI to visualize myonuclei contained within myofibers. Myonuclear numbers were significantly decreased, compared to vehicle, in myofibers of the nasal pharynx but not the oral or laryngeal pharynxes (Fig. 5G). Myonuclear loss following satellite cell ablation suggests that *Pax7⁺* satellite cells are required to maintain myonuclear numbers in nasal pharyngeal muscles.

Loss of pharyngeal satellite cells results in muscle atrophy but not fibrosis

Muscle fibrosis can occur when satellite cells are impaired, such as in aged muscles or in satellite cell-ablated hindlimb muscles following overload stress [70, 71]. Therefore, we tested whether fibrosis also occurred in the pharyngeal muscles of our satellite cell-ablated mice. Hematoxylin and eosin staining of nasal pharyngeal muscle sections revealed no obvious increase in extracellular matrix (ECM) deposition in tamoxifen-treated mice compared to vehicle (Supp. Fig. 4A). These data were confirmed using fluorescently labeled wheat germ agglutinin to visualize *N*-acetyl-D-glucosamine glycosylated ECM proteins (Supp. Fig. 4B). No significant difference in wheat germ agglutinin staining was observed between corresponding regions of the nasal pharynx of vehicle versus tamoxifen treated mice (Supp. Fig. 4C). Oral and laryngeal regions showed no differences between vehicle versus tamoxifen treated cohorts as well (data not shown). These data demonstrate that satellite cell ablation does not cause fibrosis in pharyngeal muscles.

Interestingly, myonuclear loss has been associated with muscle atrophy resulting from various stimuli [40, 62, 72, 73]. Therefore, we tested whether satellite cell ablation, which resulted in myonuclear loss, also led to pharyngeal muscle atrophy. Pharyngeal muscle sections from tamoxifen treated DTA-Pax7^{CreERTM} mice (Fig. 5E) were stained with hematoxylin/eosin and myofiber cross-sectional areas from each pharyngeal region were measured (Fig. 6A). Myofiber size was significantly decreased in satellite cell-ablated muscles of the nasal pharynx versus DTA-Pax7^{CreERTM} mice injected with vehicle (Fig. 6B). No change in myofiber size was observed in the oral or laryngeal pharynx (Fig. 6B). Importantly, muscle atrophy correlated with myonuclear loss in the nasal pharynx. These data suggest that pharyngeal satellite cells are required to maintain myofiber size in pharyngeal muscles of the nasal pharynx.

Discussion

Here we propose a novel role for satellite cells in the maintenance of pharyngeal muscles (Fig. 7). PSC are transcriptionally distinct satellite cells that contribute new myonuclei to pharyngeal myofibers through constitutive myogenesis in the absence of injury. PSC are required to maintain both pharyngeal myonuclear numbers and myofiber size, counteracting the results of active myonuclear turnover within pharyngeal muscles. As discussed below, these results give new insights into why pharyngeal muscles are affected in some muscular dystrophies yet spared in others.

Our finding that PSC proliferate under basal conditions in the absence of overt injury is in sharp contrast to the basal quiescence of satellite cells in adult hindlimb skeletal muscles [20]. Although previous groups have identified proliferative satellite cells in adult extraocular muscles (EOM), only ~1% or less of EOM satellite cells proliferate under basal conditions compared to the ~30% of PSC that proliferate in adult pharyngeal muscle [58, 59, 61]. However, a recent *in vivo* study of EOM satellite cells proposed that the proliferative phenotype observed was, in part, due to a specific highly proliferative subpopulation [74]. Our *in vitro* clonal expansion data also suggest that a subpopulation of PSC is contributing to the robust proliferative phenotype observed in pharyngeal muscle. These results are in agreement with the fact that satellite cells are a heterogenous population with differences

among cells in myogenic phenotypes [46, 75–77]. PSC are also distinct from hindlimb satellite cells at the transcriptional level. Besides expressing a unique profile of myogenic regulatory factors, PSC also express unique chemokine/cytokines compared to LSC. Interleukin-6, LIF, and monocyte chemoattractant protein-1 (MCP-1; CCL2), which were highly expressed in PSC, all stimulate myoblast proliferation through autocrine and paracrine signaling [63–65, 67–69]. This cytokine expression may drive the proliferative phenotype of PSC. Potentially, myonuclear loss may also contribute to the proliferative phenotype of PSC by directly or indirectly activating proliferative signaling pathways. For example, if nuclear material were expelled into the extracellular milieu during myonuclear turnover, nuclear molecules could induce signaling pathways, like the high-mobility group box 1 (HMGB1) and receptor for advanced glycation end-products (RAGE) pathway, that activate satellite cell proliferation [78, 79]. The potential relationship between myonuclear turnover and pharyngeal satellite cell activation is an intriguing hypothesis that warrants investigation. Further studies are needed to determine the signaling pathways and mechanisms involved in PSC activation and proliferation *in vivo*.

Proliferating PSC also progress through the myogenic lineage and contribute new myonuclei to pharyngeal muscle fibers under basal conditions. To date, only one other group of muscles, the global and orbital EOM, exhibit a similar basal state of myonuclear addition [58, 59, 61, 80, 81]. Of note, we found a correlation between satellite cell number and the incidence of satellite cell fusion with myofibers in a region-dependent manner in pharyngeal muscles. These results suggest that the increased levels of cell fusion in specific pharyngeal regions are likely due to the presence of the large resident satellite cell population rather than an increased cellular propensity for fusion. Interestingly, fusion of PSC into myofibers over a period of 16 months did not result in myonuclear accretion within pharyngeal myofibers. These findings suggested that a basal level of myonuclear loss or turnover occurs in pharyngeal muscles. To examine myonuclear turnover more directly, we ablated satellite cells *in vivo* and examined myonuclear numbers using pharyngeal muscle sections. In contrast to recent studies where satellite cell ablation did not alter myonuclear numbers in non-injured hindlimb muscles [27, 28], decreased numbers of myonuclei were observed in satellite cell-ablated muscles of the nasal pharynx. Together these data suggest that maintenance of myonuclear numbers is dependent on basal satellite cell myogenesis in pharyngeal muscles, and for the first time demonstrate myonuclear loss occurring in the absence of associated injury, disease or aging in skeletal muscle.

We also analyzed the functional outcomes of PSC ablation. A decrease in myofiber size was associated with myonuclear loss in nasopharyngeal muscles, suggesting that constitutive myonuclear addition is required to maintain nasopharyngeal muscle size. Interestingly, the muscles of the oro- and laryngopharynx possess larger numbers of activated satellite cells compared to the nasal pharynx. Despite loss of over 90% of PSC from these muscles, satellite cell numbers may have remained above a critical threshold leading to maintenance of myonuclear numbers in these regions. Another functional role of satellite cells in hindlimb muscles involves maintenance of the extracellular milieu [71]. Interestingly, we found no fibrotic changes associated with satellite cell ablation in pharyngeal muscles, suggesting that PSC may play less of a role in extracellular matrix maintenance than

recently proposed for LSC. In hindlimb skeletal muscles, satellite cells are not required for maintenance of muscle size or myonuclear number in sedentary mice [26–30]. However, our data provide evidence that satellite cells are required for maintenance of myofiber size in pharyngeal muscles and suggest that the rate of myonuclear turnover within a muscle determines whether or not the associated satellite cells are required for muscle maintenance.

To date, aging [73], muscle atrophy [72], and muscular dystrophy [82] are the major processes associated with decreases in myonuclear number, yet the molecular mechanisms that regulate myonuclear turnover remain unclear. Several groups have suggested myonuclear loss occurs in hindlimb and extraocular muscles by apoptosis using terminal deoxynucleotidyl transferase dUTP nick-end labeling (TUNEL) assays or caspase staining [62, 83, 84]. However TUNEL staining identifies DNA damage in the context of apoptosis but also necrosis and autolytic cell death pathways [85]. Alternate mechanisms such as nuclear autophagy [86, 87] or even myonuclear extrusion [88] could also contribute to myonuclear turnover. Further studies are needed to elucidate the mechanisms by which myonuclear loss occurs in pharyngeal muscles as well as why myonuclear loss occurs in these muscles.

We recently reported that both aging and disease differentially affect pharyngeal muscles dependent on their regional location within the pharynx [16]. Here we show PSC also display differential phenotypes depending on the associated muscle and its location within the pharynx. For example, the palatopharyngeus muscle extends between the nasal and oral pharynxes, yet differs in both structure and function depending on its regional location within the pharynx [16]. Interestingly, in the nasal pharynx, the palatopharyngeus consistently demonstrated the lowest number of satellite cells (both quiescent and activated) and fusion of all the pharyngeal regions examined. Additionally, the nasal palatopharyngeus was sensitive to satellite cell ablation as both myonuclear loss and decreased myofiber size occurred. This was in contrast to the palatopharyngeus of the oral pharynx, which had larger numbers of activated PSC and fusion yet demonstrated a resistance to functional changes associated with satellite cell ablation. Additionally, PSC number and fusion were greatly increased in the cricopharyngeal and thyropharyngeal muscles of the laryngeal pharynx compared to other regions of the pharynx. Together, these data suggest that differences in regional location and physiological function of pharyngeal muscles also contribute to the unique properties of PSC.

Conclusion

Our results may provide insights into why pharyngeal muscles are affected in some muscular dystrophies yet spared in others. Considering the requirement of PSC in maintenance of pharyngeal myofiber size, mutations or conditions that adversely affect PSC numbers, activation, proliferation, differentiation, or fusion could negatively impact pharyngeal muscle function. We recently observed a significant decrease in lick rates, indicative of swallowing difficulties, in a mouse model of OPMD that correlated with decreases in central myonuclear localization in pharyngeal muscles, suggesting myonuclear addition was negatively affected [16]. Additionally, some disease-causing mutations could enhance myonuclear turnover in pharyngeal muscles to such an extent that PSC could no

longer adequately supply enough myonuclei to maintain homeostasis. Aging also adversely affects pharyngeal function, resulting in impaired swallowing in 11–16% of the elderly population [89, 90]. Impairment of satellite cell function with aging [91] could contribute to this age-related increase in swallowing disorders. Further studies addressing the effects of disease and aging on both pharyngeal satellite cells and pharyngeal myonuclear turnover are warranted and could lead to new therapeutics for individuals suffering from pharyngeal myopathies.

Supplementary Material

Refer to Web version on PubMed Central for supplementary material.

Acknowledgements

We thank Drs. J.P. Canner, T. Caspary, A. English, M. Johns III, T. Lever, and R. Price for training and/or helpful discussions; E. Andreas for providing the schematic of pharyngeal anatomy; K. Carroll and N. Pescatore for technical assistance; Emory University's Integrated Genomics Core and School of Medicine Core Facility for Flow Cytometry for experimental assistance. We also thank Drs. S. Tajbakhsh and C. Keller for the generous gifts of the *Myf5^{nLacZ}+* (*Myf5* nLacZ) and *Pax7^{CreERTM}/CreERTM* (*Pax7*Cre) mice, respectively. This work was supported by National Institute of Health grants AR061987 (GP) and DC012225 (MR).

References

- Hoffman EP, Brown RH Jr, Kunkel LM. Dystrophin: the protein product of the Duchenne muscular dystrophy locus. *Cell*. 1987; 51:919–928. [PubMed: 3319190]
- Monaco AP, Bertelson CJ, Liechti-Gallati S, et al. An explanation for the phenotypic differences between patients bearing partial deletions of the DMD locus. *Genomics*. 1988; 2:90–95. [PubMed: 3384440]
- Nonaka I. Distal myopathies. *Current opinion in neurology*. 1999; 12:493–499. [PubMed: 10590885]
- Bione S, Maestrini E, Rivella S, et al. Identification of a novel X-linked gene responsible for Emery-Dreifuss muscular dystrophy. *Nat Genet*. 1994; 8:323–327. [PubMed: 7894480]
- Bonne G, Di Barletta MR, Varnous S, et al. Mutations in the gene encoding lamin A/C cause autosomal dominant Emery-Dreifuss muscular dystrophy. *Nat Genet*. 1999; 21:285–288. [PubMed: 10080180]
- Brais B, Bouchard JP, Xie YG, et al. Short GCG expansions in the PABP2 gene cause oculopharyngeal muscular dystrophy. *Nat Genet*. 1998; 18:164–167. [PubMed: 9462747]
- Robinson DO, Hammans SR, Read SP, et al. Oculopharyngeal muscular dystrophy (OPMD): analysis of the PABPN1 gene expansion sequence in 86 patients reveals 13 different expansion types and further evidence for unequal recombination as the mutational mechanism. *Hum Genet*. 2005; 116:267–271. [PubMed: 15645184]
- Godfrey C, Clement E, Mein R, et al. Refining genotype phenotype correlations in muscular dystrophies with defective glycosylation of dystroglycan. *Brain : a journal of neurology*. 2007; 130:2725–2735. [PubMed: 17878207]
- Mootosamy RC, Dietrich S. Distinct regulatory cascades for head and trunk myogenesis. *Development*. 2002; 129:573–583. [PubMed: 11830559]
- Noden DM, Francis-West P. The differentiation and morphogenesis of craniofacial muscles. *Dev Dyn*. 2006; 235:1194–1218. [PubMed: 16502415]
- Donner MW, Bosma JF, Robertson DL. Anatomy and physiology of the pharynx. *Gastrointest Radiol*. 1985; 10:196–212. [PubMed: 4029536]
- Dutta CR, Basmajian JV. Gross and histological structure of the pharyngeal constrictors in the rabbit. *Anat Rec*. 1960; 137:127–134. [PubMed: 24546072]

13. Himmelreich HA. The palatopharyngeal muscle of mammals. *Gegenbaurs Morphol Jahrb.* 1973; 119:172–212. [PubMed: 4199815]
14. Rubesin SE, Jessurun J, Robertson D, et al. Lines of the pharynx. *Radiographics.* 1987; 7:217–237. [PubMed: 3448633]
15. Miller AJ. The neurobiology of swallowing and dysphagia. *Developmental disabilities research reviews.* 2008; 14:77–86. [PubMed: 18646019]
16. Randolph ME, Luo Q, Ho J, et al. Ageing and muscular dystrophy differentially affect murine pharyngeal muscles in a region-dependent manner. *The Journal of physiology.* 2014; 592:5301–5315. [PubMed: 25326455]
17. Victor M, Hayes R, Adams RD. Oculopharyngeal muscular dystrophy. A familial disease of late life characterized by dysphagia and progressive ptosis of the eyelids. *The New England journal of medicine.* 1962; 267:1267–1272. [PubMed: 13997067]
18. Little BW, Perl DP. Oculopharyngeal muscular dystrophy. An autopsied case from the French-Canadian kindred. *J. Neurol. Sci.* 1982; 53:145–158. [PubMed: 7057207]
19. Périé S, Mamchaoui K, Mouly V, et al. Premature proliferative arrest of cricopharyngeal myoblasts in oculo-pharyngeal muscular dystrophy: Therapeutic perspectives of autologous myoblast transplantation. *Neuromuscul Disord.* 2006; 16:770–781. [PubMed: 17005403]
20. Relaix F, Zammit PS. Satellite cells are essential for skeletal muscle regeneration: the cell on the edge returns centre stage. *Development.* 2012; 139:2845–2856. [PubMed: 22833472]
21. Sacco A, Mourkioti F, Tran R, et al. Short telomeres and stem cell exhaustion model Duchenne muscular dystrophy in mdx/mTR mice. *Cell.* 2010; 143:1059–1071. [PubMed: 21145579]
22. Girgenrath M, Kostek CA, Miller JB. Diseased muscles that lack dystrophin or laminin- α 2 have altered compositions and proliferation of mononuclear cell populations. *BMC neurology.* 2005; 5:7. [PubMed: 15817132]
23. Frock RL, Kudlow BA, Evans AM, et al. Lamin A/C and emerin are critical for skeletal muscle satellite cell differentiation. *Genes Dev.* 2006; 20:486–500. [PubMed: 16481476]
24. Winokur ST, Chen YW, Masny PS, et al. Expression profiling of FSHD muscle supports a defect in specific stages of myogenic differentiation. *Hum Mol Genet.* 2003; 12:2895–2907. [PubMed: 14519683]
25. Barro M, Carnac G, Flavier S, et al. Myoblasts from affected and non-affected FSHD muscles exhibit morphological differentiation defects. *Journal of cellular and molecular medicine.* 2010; 14:275–289. [PubMed: 18505476]
26. Lepper C, Conway SJ, Fan CM. Adult satellite cells and embryonic muscle progenitors have distinct genetic requirements. *Nature.* 2009; 460:627–631. [PubMed: 19554048]
27. Jackson JR, Mula J, Kirby TJ, et al. Satellite cell depletion does not inhibit adult skeletal muscle regrowth following unloading-induced atrophy. *American journal of physiology Cell physiology.* 2012; 303:C854–C861. [PubMed: 22895262]
28. Lee SJ, Huynh TV, Lee YS, et al. Role of satellite cells versus myofibers in muscle hypertrophy induced by inhibition of the myostatin/activin signaling pathway. *Proceedings of the National Academy of Sciences of the United States of America.* 2012; 109:E2353–E2360. [PubMed: 22869749]
29. Fry CS, Lee JD, Mula J, et al. Inducible depletion of satellite cells in adult, sedentary mice impairs muscle regenerative capacity without affecting sarcopenia. *Nat Med.* 2015; 21:76–80. [PubMed: 25501907]
30. McCarthy JJ, Mula J, Miyazaki M, et al. Effective fiber hypertrophy in satellite cell-depleted skeletal muscle. *Development.* 2011; 138:3657–3666. [PubMed: 21828094]
31. Tajbakhsh S, Bober E, Babinet C, et al. Gene targeting the myf-5 locus with nlacZ reveals expression of this myogenic factor in mature skeletal muscle fibres as well as early embryonic muscle. *Dev Dyn.* 1996; 206:291–300. [PubMed: 8896984]
32. Nishijo K, Hosoyama T, Bjornson CR, et al. Biomarker system for studying muscle, stem cells, and cancer in vivo. *FASEB J.* 2009; 23:2681–2690. [PubMed: 19332644]
33. Bulfield G, Siller WG, Wight PA, et al. X chromosome-linked muscular dystrophy (mdx) in the mouse. *Proceedings of the National Academy of Sciences of the United States of America.* 1984; 81:1189–1192. [PubMed: 6583703]

34. Madisen L, Zwingman TA, Sunkin SM, et al. A robust and high-throughput Cre reporting and characterization system for the whole mouse brain. *Nature neuroscience*. 2010; 13:133–140. [PubMed: 20023653]
35. Wu S, Wu Y, Capecchi MR. Motoneurons and oligodendrocytes are sequentially generated from neural stem cells but do not appear to share common lineage-restricted progenitors in vivo. *Development*. 2006; 133:581–590. [PubMed: 16407399]
36. Mitchell PO, Pavlath GK. A muscle precursor cell-dependent pathway contributes to muscle growth after atrophy. *American journal of physiology Cell physiology*. 2001; 281:C1706–C1715. [PubMed: 11600435]
37. Bondesen BA, Mills ST, Kegley KM, et al. The COX-2 pathway is essential during early stages of skeletal muscle regeneration. *American journal of physiology Cell physiology*. 2004; 287:C475–C483. [PubMed: 15084473]
38. Yablonka-Reuveni Z, Nameroff M. Skeletal muscle cell populations. Separation and partial characterization of fibroblast-like cells from embryonic tissue using density centrifugation. *Histochemistry*. 1987; 87:27–38. [PubMed: 3038797]
39. Kafadar KA, Yi L, Ahmad Y, et al. Sca-1 expression is required for efficient remodeling of the extracellular matrix during skeletal muscle regeneration. *Dev Biol*. 2009; 326:47–59. [PubMed: 19059231]
40. Mitchell PO, Pavlath GK. Skeletal muscle atrophy leads to loss and dysfunction of muscle precursor cells. *American journal of physiology Cell physiology*. 2004; 287:C1753–C1762. [PubMed: 15329339]
41. O'Connor RS, Mills ST, Jones KA, et al. A combinatorial role for NFAT5 in both myoblast migration and differentiation during skeletal muscle myogenesis. *J Cell Sci*. 2007; 120:149–159. [PubMed: 17164296]
42. Edgar R, Domrachev M, Lash AE. Gene Expression Omnibus: NCBI gene expression and hybridization array data repository. *Nucleic Acids Res*. 2002; 30:207–210. [PubMed: 11752295]
43. Livak KJ, Schmittgen TD. Analysis of relative gene expression data using real-time quantitative PCR and the 2⁻(Delta Delta C(T)) Method. *Methods*. 2001; 25:402–408. [PubMed: 11846609]
44. Pavlath GK, Thaloer D, Rando TA, et al. Heterogeneity among muscle precursor cells in adult skeletal muscles with differing regenerative capacities. *Dev Dyn*. 1998; 212:495–508. [PubMed: 9707323]
45. Sambasivan R, Gayraud-Morel B, Dumas G, et al. Distinct regulatory cascades govern extraocular and pharyngeal arch muscle progenitor cell fates. *Dev Cell*. 2009; 16:810–821. [PubMed: 19531352]
46. Ono Y, Boldrin L, Knopp P, et al. Muscle satellite cells are a functionally heterogeneous population in both somite-derived and branchiomic muscles. *Dev Biol*. 2010; 337:29–41. [PubMed: 19835858]
47. Cooper RN, Tajbakhsh S, Mouly V, et al. In vivo satellite cell activation via Myf5 and MyoD in regenerating mouse skeletal muscle. *J Cell Sci*. 1999; 112(Pt 17):2895–2901. [PubMed: 10444384]
48. Beauchamp JR, Heslop L, Yu DS, et al. Expression of CD34 and Myf5 defines the majority of quiescent adult skeletal muscle satellite cells. *The Journal of cell biology*. 2000; 151:1221–1234. [PubMed: 11121437]
49. Seale P, Sabourin LA, Girgis-Gabardo A, et al. Pax7 is required for the specification of myogenic satellite cells. *Cell*. 2000; 102:777–786. [PubMed: 11030621]
50. Gidaro T, Negroni E, Périé S, et al. Atrophy, fibrosis, and increased PAX7-positive cells in pharyngeal muscles of oculopharyngeal muscular dystrophy patients. *J. Neuropathol. Exp. Neurol*. 2013; 72:234–243. [PubMed: 23399899]
51. Blanco-Bose WE, Yao CC, Kramer RH, et al. Purification of mouse primary myoblasts based on alpha 7 integrin expression. *Exp Cell Res*. 2001; 265:212–220. [PubMed: 11302686]
52. Cornelison DD, Filla MS, Stanley HM, et al. Syndecan-3 and syndecan-4 specifically mark skeletal muscle satellite cells and are implicated in satellite cell maintenance and muscle regeneration. *Dev Biol*. 2001; 239:79–94. [PubMed: 11784020]

53. Asakura A, Seale P, Girgis-Gabardo A, et al. Myogenic specification of side population cells in skeletal muscle. *The Journal of cell biology*. 2002; 159:123–134. [PubMed: 12379804]
54. Tamaki T, Akatsuka A, Ando K, et al. Identification of myogenic-endothelial progenitor cells in the interstitial spaces of skeletal muscle. *The Journal of cell biology*. 2002; 157:571–577. [PubMed: 11994315]
55. Sherwood RI, Christensen JL, Conboy IM, et al. Isolation of adult mouse myogenic progenitors: functional heterogeneity of cells within and engrafting skeletal muscle. *Cell*. 2004; 119:543–554. [PubMed: 15537543]
56. Fukada S, Uezumi A, Ikemoto M, et al. Molecular signature of quiescent satellite cells in adult skeletal muscle. *Stem cells*. 2007; 25:2448–2459. [PubMed: 17600112]
57. Ikemoto M, Fukada S, Uezumi A, et al. Autologous transplantation of SM/C-2.6(+) satellite cells transduced with micro-dystrophin CS1 cDNA by lentiviral vector into mdx mice. *Molecular therapy : the journal of the American Society of Gene Therapy*. 2007; 15:2178–2185. [PubMed: 17726457]
58. McLoon LK, Wirtschafter J. Activated satellite cells are present in uninjured extraocular muscles of mature mice. *Transactions of the American Ophthalmological Society*. 2002; 100:119–123. discussion 123–114. [PubMed: 12545684]
59. McLoon LK, Wirtschafter J. Activated satellite cells in extraocular muscles of normal adult monkeys and humans. *Invest Ophthalmol Vis Sci*. 2003; 44:1927–1932. [PubMed: 12714625]
60. McLoon LK, Thorstenson KM, Solomon A, et al. Myogenic precursor cells in craniofacial muscles. *Oral diseases*. 2007; 13:134–140. [PubMed: 17305613]
61. Stuelsatz P, Shearer A, Li Y, et al. Extraocular muscle satellite cells are high performance myo-engines retaining efficient regenerative capacity in dystrophin deficiency. *Dev Biol*. 2015; 397:31–44. [PubMed: 25236433]
62. Dupont-Versteegden EE, Murphy RJ, Houle JD, et al. Activated satellite cells fail to restore myonuclear number in spinal cord transected and exercised rats. *The American journal of physiology*. 1999; 277:C589–C597. [PubMed: 10484346]
63. Spangenburg EE, Booth FW. Multiple signaling pathways mediate LIF-induced skeletal muscle satellite cell proliferation. *American journal of physiology Cell physiology*. 2002; 283:C204–C211. [PubMed: 12055089]
64. Serrano AL, Baeza-Raja B, Perdiguero E, et al. Interleukin-6 is an essential regulator of satellite cell-mediated skeletal muscle hypertrophy. *Cell metabolism*. 2008; 7:33–44. [PubMed: 18177723]
65. Yahiaoui L, Gvozdic D, Danialou G, et al. CC family chemokines directly regulate myoblast responses to skeletal muscle injury. *The Journal of physiology*. 2008; 586:3991–4004. [PubMed: 18566004]
66. Griffin CA, Apponi LH, Long KK, et al. Chemokine expression and control of muscle cell migration during myogenesis. *J Cell Sci*. 2010; 123:3052–3060. [PubMed: 20736301]
67. Broholm C, Laye MJ, Brandt C, et al. LIF is a contraction-induced myokine stimulating human myocyte proliferation. *Journal of applied physiology*. 2011; 111:251–259. [PubMed: 21527666]
68. Henningsen J, Pedersen BK, Kratchmarova I. Quantitative analysis of the secretion of the MCP family of chemokines by muscle cells. *Molecular bioSystems*. 2011; 7:311–321. [PubMed: 21152491]
69. Toth KG, McKay BR, De Lisio M, et al. IL-6 induced STAT3 signalling is associated with the proliferation of human muscle satellite cells following acute muscle damage. *PLoS One*. 2011; 6:e17392. [PubMed: 21408055]
70. Brack AS, Conboy MJ, Roy S, et al. Increased Wnt signaling during aging alters muscle stem cell fate and increases fibrosis. *Science*. 2007; 317:807–810. [PubMed: 17690295]
71. Fry CS, Lee JD, Jackson JR, et al. Regulation of the muscle fiber microenvironment by activated satellite cells during hypertrophy. *FASEB J*. 2014; 28:1654–1665. [PubMed: 24376025]
72. Hikida RS, Van Nostran S, Murray JD, et al. Myonuclear loss in atrophied soleus muscle fibers. *The Anatomical record*. 1997; 247:350–354. [PubMed: 9066912]
73. Brack AS, Bildsoe H, Hughes SM. Evidence that satellite cell decrement contributes to preferential decline in nuclear number from large fibres during murine age-related muscle atrophy. *J Cell Sci*. 2005; 118:4813–4821. [PubMed: 16219688]

74. Kallestad KM, Hebert SL, McDonald AA, et al. Sparing of extraocular muscle in aging and muscular dystrophies: a myogenic precursor cell hypothesis. *Exp Cell Res.* 2011; 317:873–885. [PubMed: 21277300]
75. Tanaka KK, Hall JK, Troy AA, et al. Syndecan-4-expressing muscle progenitor cells in the SP engraft as satellite cells during muscle regeneration. *Cell Stem Cell.* 2009; 4:217–225. [PubMed: 19265661]
76. Alfaro LA, Dick SA, Siegel AL, et al. CD34 promotes satellite cell motility and entry into proliferation to facilitate efficient skeletal muscle regeneration. *Stem cells.* 2011; 29:2030–2041. [PubMed: 21997891]
77. Rocheteau P, Gayraud-Morel B, Siegl-Cachedenier I, et al. A subpopulation of adult skeletal muscle stem cells retains all template DNA strands after cell division. *Cell.* 2012; 148:112–125. [PubMed: 22265406]
78. Sims GP, Rowe DC, Rietdijk ST, et al. HMGB1 and RAGE in inflammation and cancer. *Annual review of immunology.* 2010; 28:367–388.
79. Riuzzi F, Sorci G, Sgheddu R, et al. HMGB1-RAGE regulates muscle satellite cell homeostasis through p38-MAPK- and myogenin-dependent repression of Pax7 transcription. *J Cell Sci.* 2012; 125:1440–1454. [PubMed: 22328527]
80. McLoon LK, Wirtschafter JD. Continuous myonuclear addition to single extraocular myofibers in uninjured adult rabbits. *Muscle Nerve.* 2002; 25:348–358. [PubMed: 11870711]
81. Wirtschafter JD, Ferrington DA, McLoon LK. Continuous remodeling of adult extraocular muscles as an explanation for selective craniofacial vulnerability in oculopharyngeal muscular dystrophy. *Journal of neuro-ophthalmology : the official journal of the North American Neuro-Ophthalmology Society.* 2004; 24:62–67. [PubMed: 15206442]
82. Mittelbronn M, Sullivan T, Stewart CL, et al. Myonuclear degeneration in LMNA null mice. *Brain pathology.* 2008; 18:338–343. [PubMed: 18371185]
83. Adhihetty PJ, O'Leary MF, Chabi B, et al. Effect of denervation on mitochondrially mediated apoptosis in skeletal muscle. *Journal of applied physiology.* 2007; 102:1143–1151. [PubMed: 17122379]
84. McLoon LK, Rowe J, Wirtschafter J, et al. Continuous myofiber remodeling in uninjured extraocular myofibers: myonuclear turnover and evidence for apoptosis. *Muscle Nerve.* 2004; 29:707–715. [PubMed: 15116375]
85. Grasl-Kraupp B, Ruttka-Nedecky B, Koudelka H, et al. In situ detection of fragmented DNA (TUNEL assay) fails to discriminate among apoptosis, necrosis, and autolytic cell death: a cautionary note. *Hepatology.* 1995; 21:1465–1468. [PubMed: 7737654]
86. Park YE, Hayashi YK, Bonne G, et al. Autophagic degradation of nuclear components in mammalian cells. *Autophagy.* 2009; 5:795–804. [PubMed: 19550147]
87. Mijaljica D, Prescott M, Devenish RJ. The intricacy of nuclear membrane dynamics during nucleophagy. *Nucleus.* 2010; 1:213–223. [PubMed: 21327066]
88. Runge MS, Stouffer GA, Sheahan RG, et al. Morphological patterns of death by myocytes in arrhythmogenic right ventricular dysplasia. *The American journal of the medical sciences.* 2000; 320:310–319. [PubMed: 11093683]
89. Kawashima K, Motohashi Y, Fujishima I. Prevalence of dysphagia among community-dwelling elderly individuals as estimated using a questionnaire for dysphagia screening. *Dysphagia.* 2004; 19:266–271. [PubMed: 15667063]
90. Holland G, Jayasekeran V, Pendleton N, et al. Prevalence and symptom profiling of oropharyngeal dysphagia in a community dwelling of an elderly population: a self-reporting questionnaire survey. *Diseases of the esophagus : official journal of the International Society for Diseases of the Esophagus / ISDE.* 2011; 24:476–480.
91. Brack AS, Rando TA. Intrinsic changes and extrinsic influences of myogenic stem cell function during aging. *Stem cell reviews.* 2007; 3:226–237. [PubMed: 17917136]

Significance Statement

Pharyngeal muscles are essential for swallowing and are preferentially affected in some muscular dystrophies yet spared in others. Muscle stem cells, called satellite cells, may be critical factors in the development of pharyngeal muscle disorders; however, very little is known about pharyngeal satellite cells (PSC) and their role in pharyngeal muscles. Here we characterize satellite cells of pharyngeal muscles demonstrating that pharyngeal satellite cells undergo myogenesis under basal conditions. Additionally, PSC are required for maintenance of both pharyngeal myofiber size and myonuclear number, suggesting that satellite cell impairment could contribute to pharyngeal myopathies.

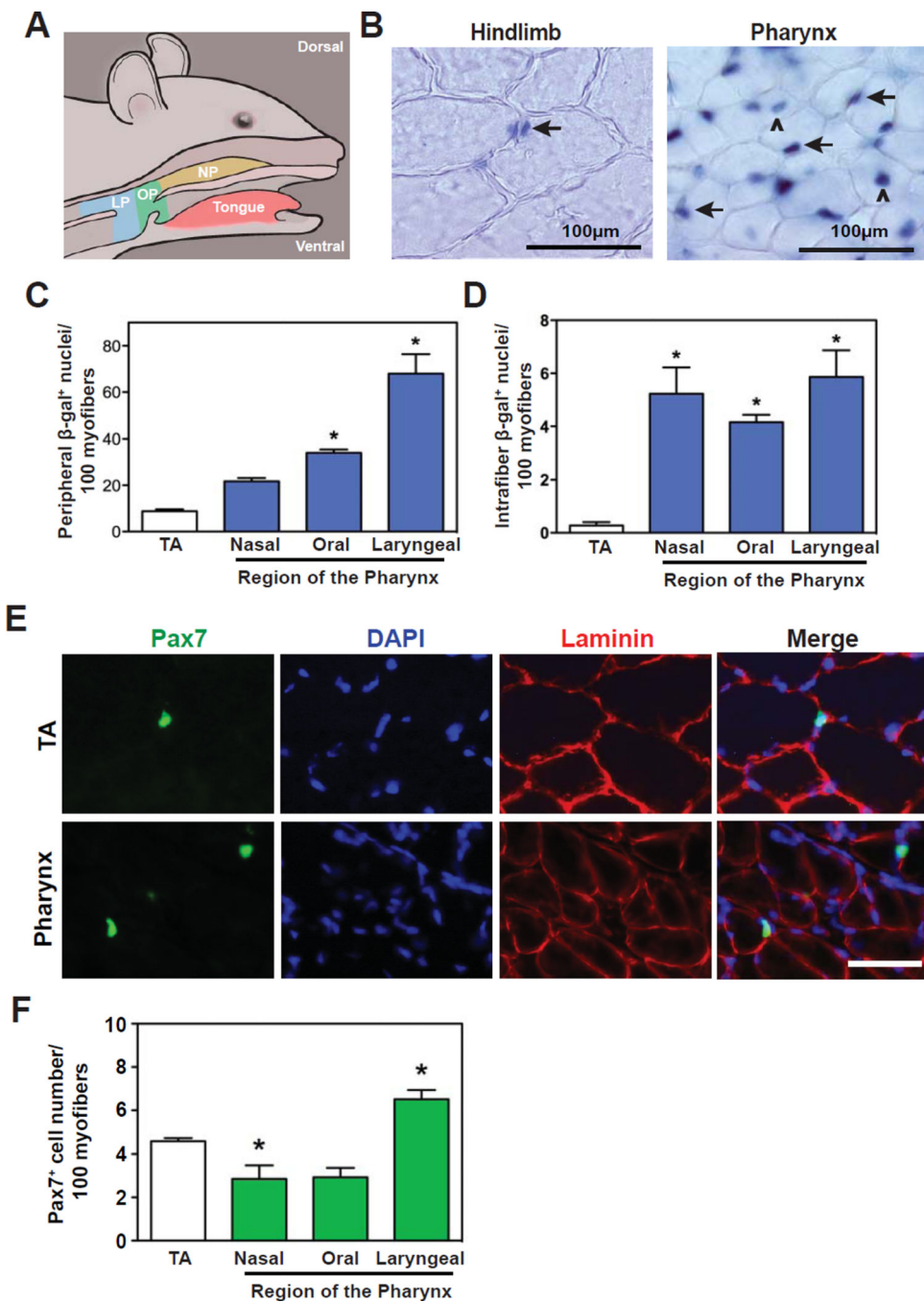


Figure 1. Pharyngeal muscles contain a larger number of activated satellite cells than hindlimb muscle

(A) Schematic of murine pharyngeal regions: NP = nasal pharynx; OP = oral pharynx; LP = laryngopharynx. (Modified from Randolph *et al.*, 2014.) (B) Hindlimb (tibialis anterior) and pharyngeal muscles were collected at nine weeks of age from Myf5-nlacZ mice, sectioned, and incubated with X-gal to identify β -gal⁺ nuclei (blue). Representative muscle sections from hindlimb and oral pharynx (palatopharyngeus) are shown. Two types of β -gal⁺ nuclei were observed: peripherally located to myofibers (arrows) or centrally located within myofibers (Δ). (C) Each pharyngeal region contained increased numbers of peripherally

located β -gal⁺ nuclei (satellite cells) versus hindlimb muscle. (D) Increased numbers of centrally localized β -gal⁺ myonuclei in myofibers were also observed in each pharyngeal region relative to hindlimb muscle. Data in C and D represent the mean \pm SEM. * $p < 0.05$. $n=4$ mice. (E,F) Representative muscle sections from 8–9 week old C57BL/6 mice immunostained for Pax7 (green) and laminin (red). Pax7⁺ cells colocalizing with DAPI and laminin were identified (E) and quantified (F). Bar = 100 μ m. Data represent the mean \pm SEM. * $p < 0.05$. $n=4$ mice. TA= tibialis anterior muscle.

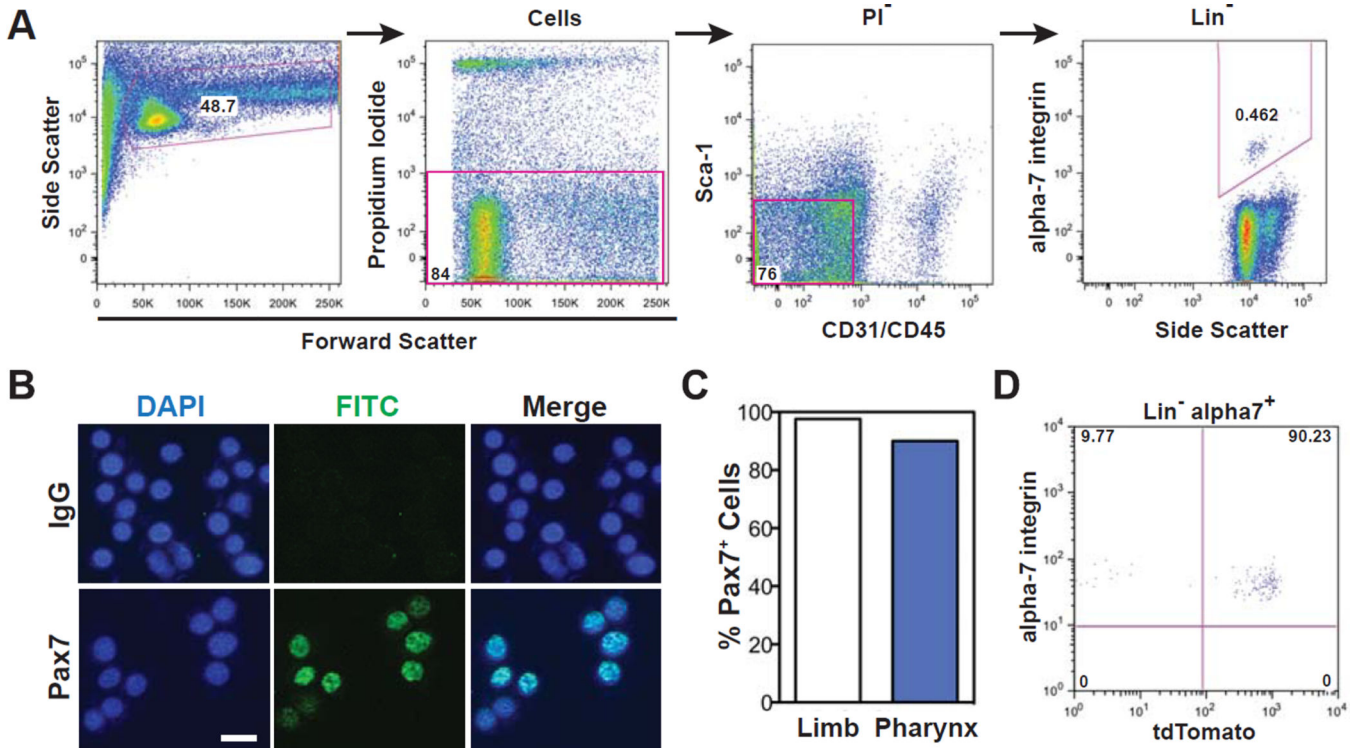


Figure 2. Identification of pharyngeal satellite cells using established cellular markers for hindlimb satellite cells
 (A) Flow cytometry gating to identify and sort satellite cells isolated from pharyngeal muscle. Pharyngeal satellite cells were identified as $\alpha 7$ -Integrin⁺ cells not derived from endothelial (CD31), hematopoietic (CD45), or fibro-adipogenic progenitor (Sca1) lineages (Lin⁻ $\alpha 7$ -Integrin⁺). (B,C) Lin⁻ $\alpha 7$ -Integrin⁺ cells were sorted and Pax7 expression visualized (B) and quantitated (C) *in vitro* using immunofluorescence. n= 509 pooled cells from 2 experiments of 10 mice each. (D) Approximately 90% of pharyngeal Lin⁻ $\alpha 7$ -Integrin⁺ cells were tdTomato⁺ following tamoxifen-treatment of *Pax7^{CreERTM}/Rosa^{tdTomato}* heterozygotes. n=2 experiments of 2–3 mice pooled. PI = propidium iodide. Bar=20 μ m.

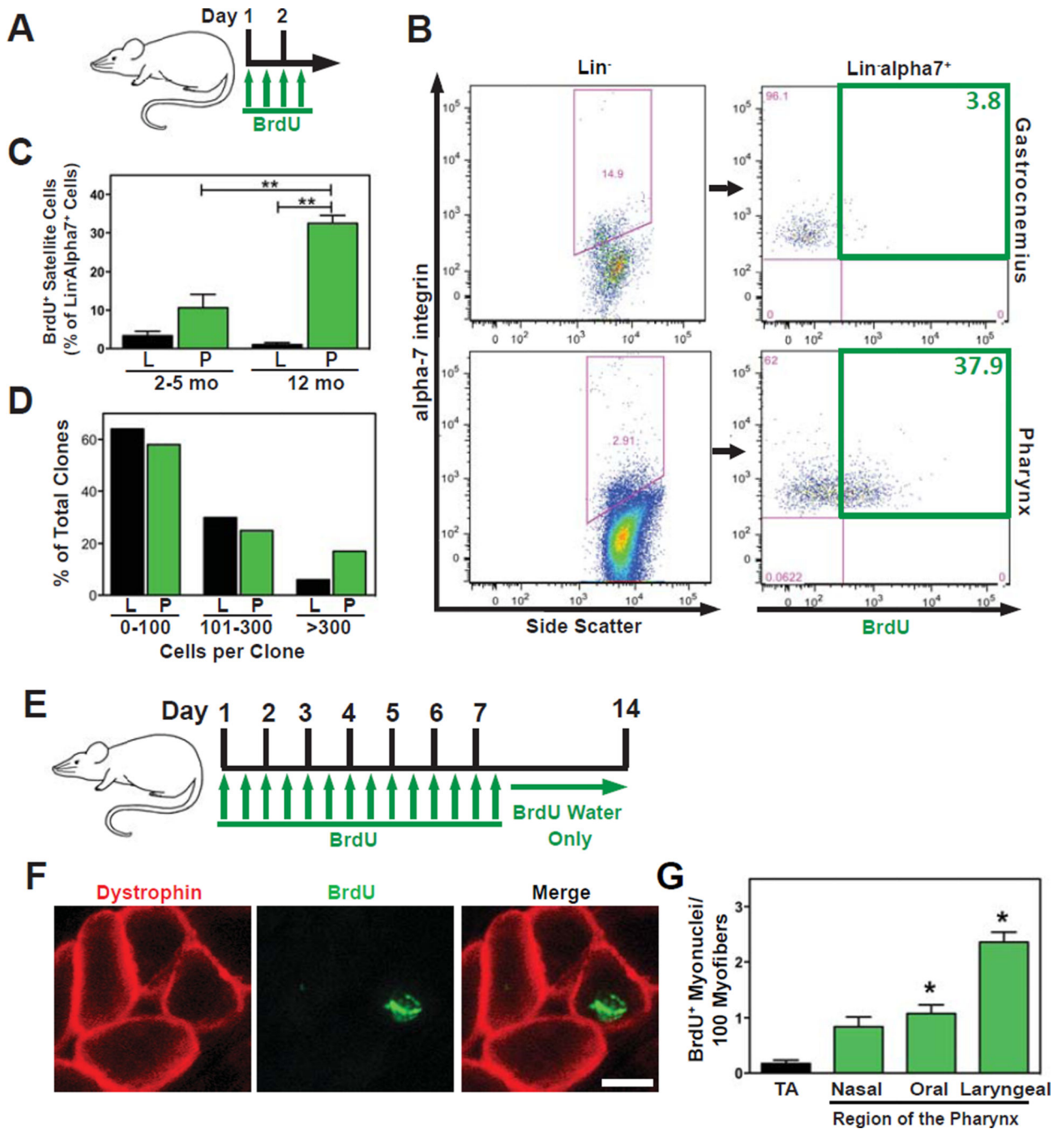


Figure 3. Pharyngeal satellite cells proliferate and fuse with pharyngeal myofibers in the absence of induced injury

(A) Schematic of BrdU treatment protocol. (B) $\text{PI}^- \text{CD}31^- \text{CD}45^- \text{Sca}1^- \alpha 7\text{-Integrin}^+$ ($\text{Lin}^- \alpha 7\text{-Integrin}^+$) satellite cells were identified using flow cytometry (left column) and analyzed to determine the percentage of proliferating satellite cells (BrdU^+) in each tissue (right column). $n=3$ mice pooled. (C) Quantification of $\text{BrdU}^+ \text{Lin}^- \alpha 7\text{-Integrin}^+$ cells demonstrated a significantly larger proliferating population of satellite cells in pharyngeal versus hindlimb (gastrocnemius) muscles. Data represent the mean \pm SEM. $^{***}p < 0.0001$, $n=3$ experiments, 3–5 mice per experiment. (D) $\text{Lin}^- \alpha 7\text{-Integrin}^+$ cells from either hindlimb

(gastrocnemius/quadriceps) or pharyngeal muscles were sorted, plated at clonal densities and cultured for 8 days. Cultures were then fixed and stained with hematoxylin for quantification of cell number per clone. The number of large clones (>300 cells) was increased three-fold in pharyngeal versus hindlimb cultures. n=264 clones from 2 experiments using 10 mice each. (E) Schematic of BrdU treatment protocol. (F) Muscle sections were immunostained for dystrophin (red) and BrdU (green). BrdU⁺ nuclei contained within a dystrophin⁺ myofiber outline represent satellite cells that recently proliferated and fused into myofibers. Bar=50 μ m. (G) Satellite cell fusion was quantified as the number of intrafiber BrdU⁺ nuclei per 100 myofibers. Satellite cell fusion occurred with higher frequency in pharyngeal muscles compared to hindlimb muscles. *p < 0.05, n=4 mice. L=hindlimb. P=pharynx. TA=tibialis anterior.

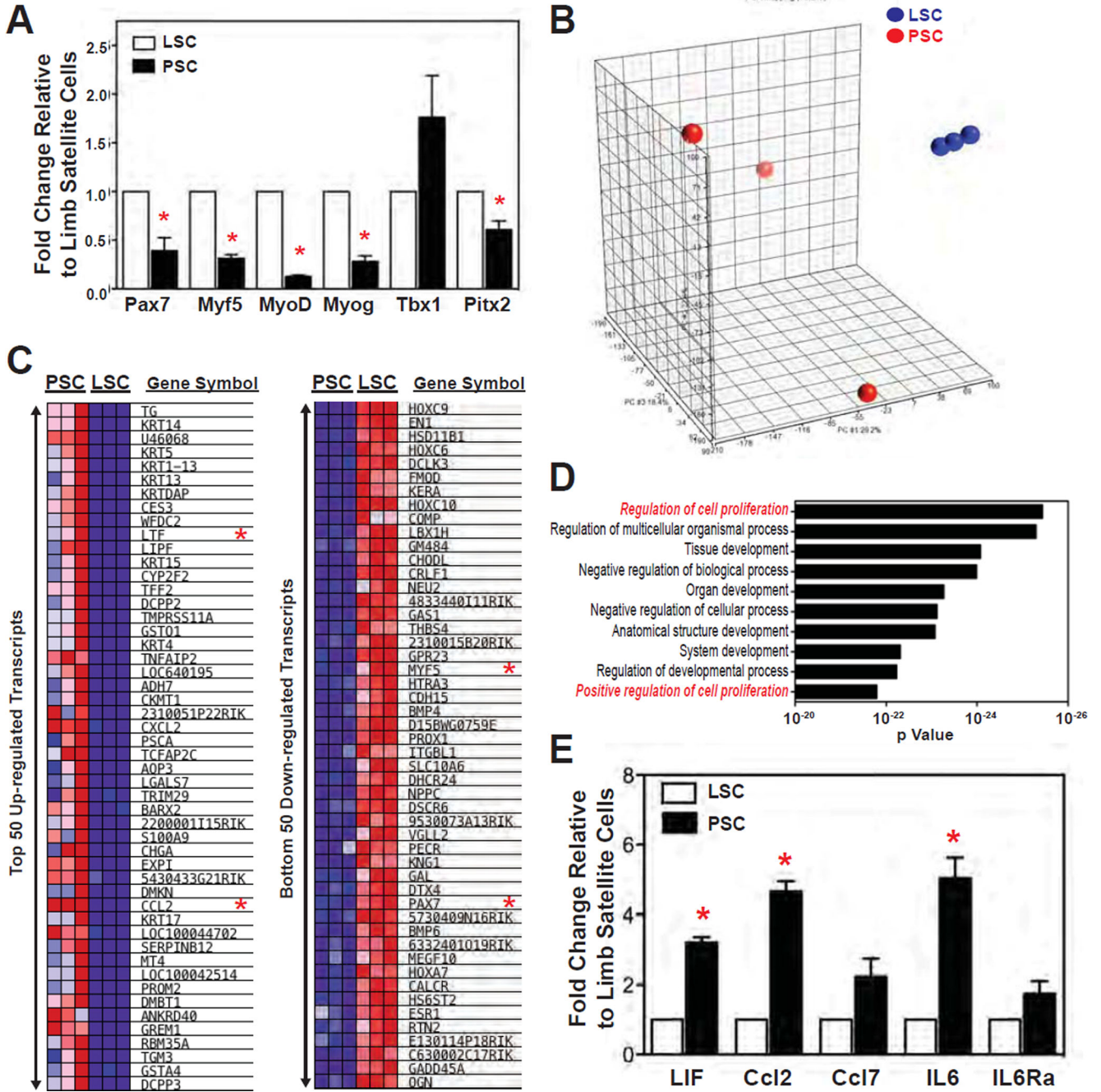


Figure 4. Comparative transcriptome analyses reveal pharyngeal and hindlimb satellite cells are distinct

Gene-expression analyses of FACS sorted pharyngeal and hindlimb satellite cells as determined by qRT-PCR (A,E) and microarray (B–D). (A) Selected regulatory transcripts involved in myogenesis were analyzed via qRT-PCR using RNA isolated from FACS sorted PSC and LSC. Data represent the mean fold-change of transcript steady-state levels \pm SEM. $n=3$ experiments each containing 150,000–200,000 satellite cells pooled from 10–30 mice. * $P<0.05$. (B) Principal component analysis (PCA) of pharyngeal satellite cells (PSC, red dots) versus hindlimb (gastrocnemius/quadriceps) satellite cells (LSC, blue dots). PCA

coordinates (PC1, 29.2%; PC2, 22.6%; and PC3, 18.4%) revealed a total data variation of 70.2%. n=3 experiments each containing 200,000 satellite cells pooled from 10–30 mice. (C) Heat maps comparing the levels of the top 50 transcripts either up- or down-regulated in PSC relative to LSC. Steady-state RNA levels are represented with a linear color scale ranging from dark red (enriched) to dark blue (depleted). Transcripts marked with red asterisks were validated by qRT-PCR. (D) Gene ontology (GO) process networks enriched in PSC generated with MetaCore Genego software. GO networks related to cell proliferation are highlighted in red. (E) qRT-PCR was used to validate microarray data of selected cytokine/chemokine transcripts that were enriched in PSC relative to LSC. Data represent the mean fold-change of transcript steady-state levels \pm SEM. n=3 hindlimb and 4–5 pharyngeal experiments each containing 1500,000–200,000 satellite cells pooled from 10–30 mice. *P<0.05.

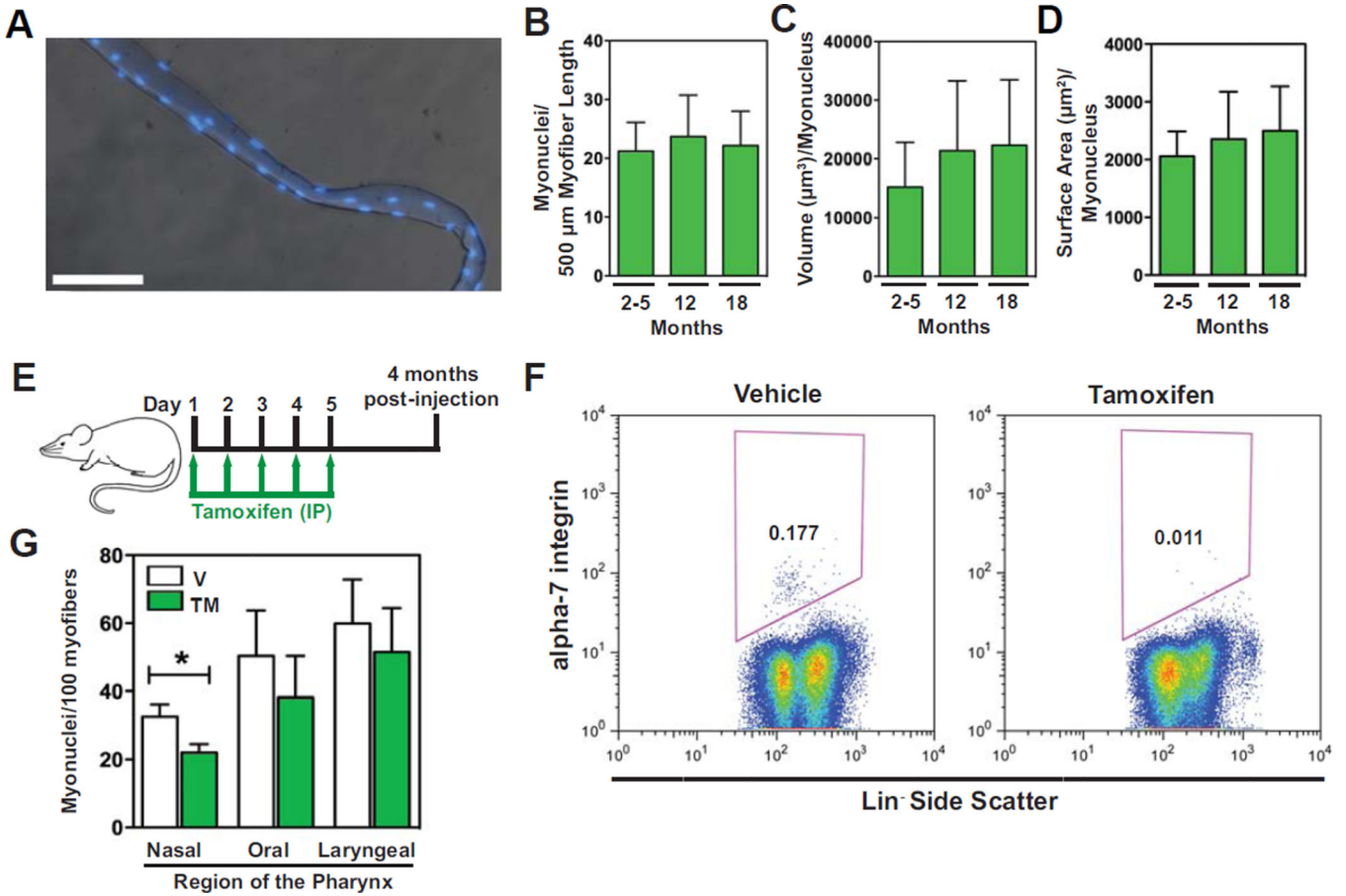


Figure 5. Myonuclear turnover occurs in pharyngeal muscle under basal conditions
 (A) Merged DAPI and phase contrast images of a representative myofiber isolated from pharyngeal muscles. Bar=50μm. (B–D) Quantification of various pharyngeal myonuclear parameters indicated no change in myonuclear numbers with age. n=26–35 fibers per timepoint. (E) Schematic of satellite cell-specific ablation in *Pax7^{CreERTM}/Rosa^{DTA-176}* heterozygous mice. (F) Pharyngeal Lin⁻ α7-Integrin⁺ cells were ablated following tamoxifen-treatment of *Pax7^{CreERTM}/Rosa^{DTA-176}* (DTA/*Pax7^{CreERTM}*) heterozygotes. Ablation efficiencies for pharyngeal Lin⁻ α7-Integrin⁺ cells ranged from 87–97%. n=8 experiments of 2–3 mice pooled. (G) Quantification of DAPI⁺ nuclei contained within dystrophin⁺ myofiber outlines revealed myonuclear loss within satellite cell-ablated muscles of the nasal pharynx. *p<0.05, n=3–4 mice per condition.

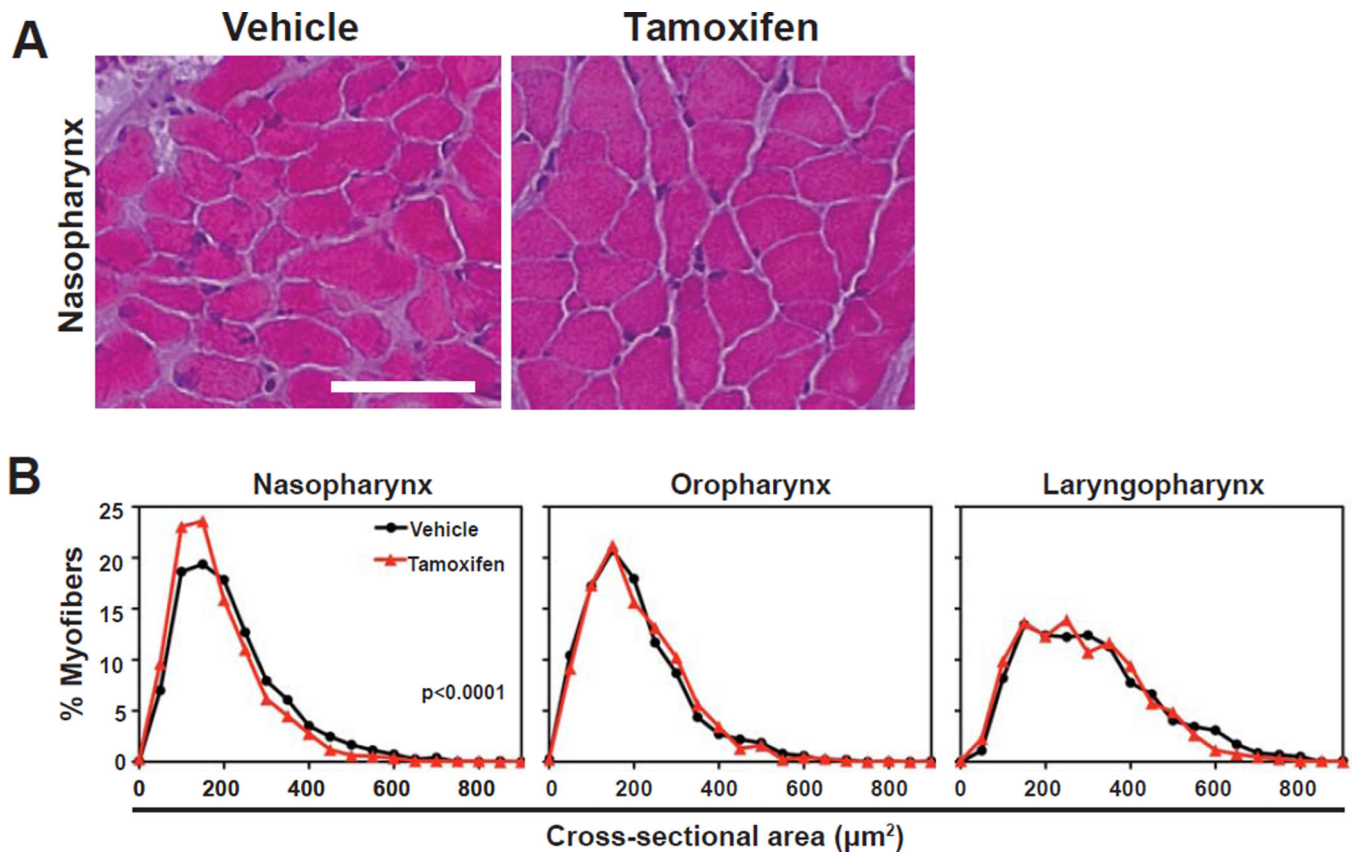


Figure 6. Pharyngeal satellite cells are required to prevent muscle atrophy in the nasal and laryngeal pharynxes

DTA/Pax7^{CreERTM} mice received either vehicle or tamoxifen injections as described in Fig. 5E with pharyngeal muscles collected 4-months post-treatment. (A) Histologic sections of vehicle and tamoxifen treated mice. Bar=50 μm . (B) Frequency distribution plots of myofiber cross-sectional areas from the naso-, oro-, and laryngopharyngeal regions are shown. Myofiber size of nasal pharyngeal muscles decreased following satellite cell ablation. n=929–1505 myofibers, 3 mice per condition.

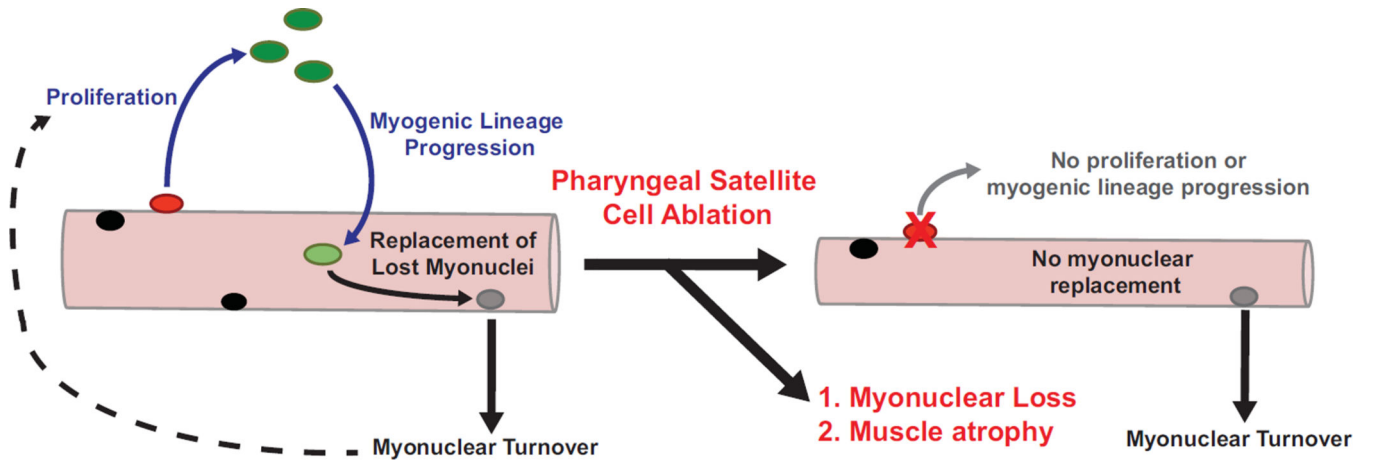


Figure 7. Model of basal pharyngeal satellite cell biology and maintenance of myofiber size
 Pharyngeal satellite cells (red) proliferate, progress through myogenesis, and contribute myonuclei (black) to pharyngeal myofibers under basal conditions. The continual contribution of new myonuclei (light green) to pharyngeal myofibers counteracts the basal myonuclear loss (grey), preventing both loss of myonuclear numbers and myofiber size. Pharyngeal satellite cell impairment reduces myonuclear addition to pharyngeal myofibers resulting in both myonuclear loss and decreased myofiber size.